Journal of Macromolecular Science, Part A
Publication details, including instructions for authors and subscription information:
http://www.informaworld.com/smpp/title~content=t713597274

Isoregic Thienylene-Phenylene Polymers: The Effects of Structural Variation and Application to Photovoltaic Devices

Young-gi kim[a]; Emilie M. Galand[a]; Barry C. Thompson[a]; John walker[b]; Stephen A. Fossey[b]; Tracy D. Mccarley[c]; Khalil A. Abboud[a]; John R. Reynolds[a]
[a] The George and Josephine Butler Polymer Research Laboratories, Department of Chemistry, Center for Macromolecular Science and Engineering, University of Florida, Gainesville, Florida [b] Natick Soldier Center, US Army Soldier and Biological Chemical Command, Natick, MA [c] Department of Chemistry, Louisiana State University, Baton Rouge, Louisiana

To cite this Article kim, Young-gi , Galand, Emilie M. , Thompson, Barry C. , walker, John , Fossey, Stephen A. , Mccarley, Tracy D. , Abboud, Khalil A. and Reynolds, John R.(2007) 'Isoregic Thienylene-Phenylene Polymers: The Effects of Structural Variation and Application to Photovoltaic Devices', Journal of Macromolecular Science, Part A, 44: 7, 665 — 674
To link to this Article: DOI: 10.1080/10601320701350906
URL: http://dx.doi.org/10.1080/10601320701350906

Journal of Macromolecular Science ®, Part A: Pure and Applied Chemistry (2007) **44**, 665–674

ISSN: 1060-1325 print / 1520-5738 online
DOI: 10.1080/10601320701350906

Isoregic Thienylene-Phenylene Polymers: The Effects of Structural Variation and Application to Photovoltaic Devices

YOUNG-GI KIM,[1] EMILIE M. GALAND,[1] BARRY C. THOMPSON,[1†] JOHN WALKER,[2] STEPHEN A. FOSSEY,[2] TRACY D. MCCARLEY,[3] KHALIL A. ABBOUD,[1] and JOHN R. REYNOLDS[1]

[1]*The George and Josephine Butler Polymer Research Laboratories, Department of Chemistry, Center for Macromolecular Science and Engineering, University of Florida, Gainesville, Florida*
[2]*Natick Soldier Center, US Army Soldier and Biological Chemical Command, Natick, MA*
[3]*Department of Chemistry, Louisiana State University, Baton Rouge, Louisiana*

Received and accepted February, 2007

Isoregic conjugated polymers composed of thiophene and dialkoxybenzene units were designed to harvest incident light in the mid-visible energy range (band gap of 2.1 eV). Poly(1,4-bis(2-thienyl)-2,5-diheptoxybenzene) (PBTB(OC_7H_{15})$_2$) and poly(1,4-bis(2-thienyl)-2,5-didodecyloxybenzene) (PBTB($OC_{12}H_{25}$)$_2$) have shown significant photovoltaic performance as an electron donor when used in tandem with the electron acceptor [6, 6]-phenyl C_{61}-butyric acid methyl ester (PCBM) in bulk hetero-junction photovoltaic devices. Photovoltaic devices incorporating PBTB(OC_7H_{15})$_2$ and PCBM have shown AM1.5 efficiencies of ~0.6% with a short circuit current density of 2.5 mA/cm^2, an open circuit voltage of 0.74 V, and a fill factor of 0.32. Incident Photon-to-Current Efficiency (IPCE) of the device was found to be *ca.* 16% at 410 nm. In order to examine the relationship between the molecular structure of the polymers and their electronic energy levels, and to correlate this with photovoltaic performance, optoelectronic and electrochemical results are discussed in relation to the I-V characteristics of the devices. Additionally, a computer-aided simulation is used to gain further insight into the effect of polymer structure on the energetic relationships in the bulk heterojunction devices.

Keywords: PCBM; band gap; solar cells; photovoltaic devices; conjugated polymer; electrochemistry; spectroelectrochemistry

1 Introduction

Organic electronics have attracted great interest due to the optimistic forecast for achieving light weight and flexible devices. Applications in various areas are being explored, including field effect transistors (FETs), (1, 2) non volatile memories (NVMs), (3) batteries, (4) supercapacitors (SCs), (5) photovoltaic devices (PVDs), (6–8) light emitting diodes (LEDs) (9) and electrochromic devices (ECDs) (10). The discovery of photoactivity in conjugated polymers in particular, (11) has triggered a major research effort over the past decade, resulting in great advances in the field (12). Overall, it is the possibility of structurally modulating the optoelectronic properties of conjugated polymers, that has continued to drive the growth of interest in the field.

The structural control of electronic properties, namely the magnitude of the band gap, has been discussed extensively in the literature (13). The band gap of a given polymer is a critical parameter for the operation of a PV device and approaches have been taken to synthesize polymers with precisely defined energy levels for optimal solar cell operation, (14) ensuring effective light absorption and alignment of energy levels. Another critical parameter that can be controlled via structural variation is the long-range order or crystallinity in a polymer or polymer blend film. Structural features that foster long range order include a high degree of regioregularity, as has been specifically important for the development of highly efficient poly(3-hexylthiophene) (P3HT) solar cells, (15) as semi-crystalline P3HT has a broader absorption spectrum and higher hole mobility than its regio-irregular and amorphous analogue. The judicious application of thermal annealing treatments has been found to be especially useful for enhancing polymer crystallinity.

While much effort has been devoted to the synthesis of regioregular polythiophenes as a means of achieving polymers capable of a high degree of crystallinity, perhaps

†Current address: Department of Chemistry, University of California Berkeley, CA.
Address correspondence to: John R. Reynolds, The George and Josephine Butler Polymer Research Laboratories, Department of Chemistry, Center for Macromolecular Science and Engineering, University of Florida, Gainesville, FL 32611. E-mail: reynolds@chem.ufl.edu

a more attractive route is the synthesis of regiosymmetric polymers which can achieve a high degree of order without the need to synthesize unsymmetrical monomers or rely on highly controlled polymerization conditions. The use of symmetrically derivatized poly(3,4-propylenedioxythiophenes) has exemplified the development of regiosymmetric conjugated polymers (16). Similarly, a regiosymmetric alternating polymer based on EDOT and dialkoxybenzene was found to give interesting electrochromic properties (17). J. Ruiz et al. and Z. Bao et al. utilized oxidation with ferric chloride and Stille coupling respectively, for synthesizing regiosymmetric conjugated polymers based on thiophene and phenylene moieties (18, 19). As shown in Scheme 1, the isoregic conformational isomer of poly(1,4-bis(2-thienyl)-2,5-didodecyloxyphenylene) has an advantage over the aregic form to facilitate molecular stacking via interweaving of side chains in a regular pattern. The work by J. Ruiz et al. revealed that poly(1,4-bis(2-thienyl)-2,5-didodecyloxy phenylene) showed an X-ray diffraction pattern that indicated a high crystalline content relative to analogous polymers having side chains of different lengths. Regiosymmetric polymers built with thiophene and phenylene moieties have a band gap somewhat larger than P3HT (2.1 eV vs. 1.9 eV) and based on their ability to give polymer films with a high degree of order, these polymers are of interest for use in solar cells.

Here, we present the synthesis, characterization, and application of two isoregic conjugated polymers with varied side-chain length in PV devices. For the polymerization, the Yamamoto coupling reaction was applied using $Ni(COD)_2$ (20). The relationship between the electronic band structure and the photovoltaic performance, along with variation in molecular structure of the resultant conjugated polymers, is discussed in order to address a strategy for the fabrication of efficient polymer-based PVDs.

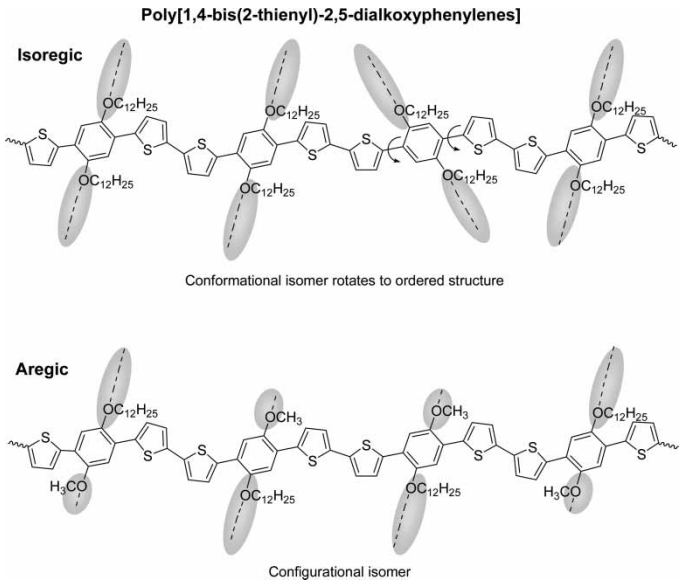

Sch. 1. Chemical structures of conformational and configurational isomers of poly(1,4-bis(2-thienyl)-2,5-dialkoxyphenylenes).

2 Experimental

2.1 General

Details on materials used along with synthesis and structural characterization are given. GPC was performed on two 300 × 7.5 mm Polymer Laboratories PLGel 5 μM mixed-C columns with Waters Associates liquid chromatography 2996 photodiode array absorption. Polymer solutions were prepared in THF and filtered through a 50 μM filter before injection. A constant flow rate of 1 mL/min was used. Molecular weights were obtained relative to polystyrene standards (Polymer Laboratories, S-M2-10 lot 30). Molar mass of the repeat units was measured by matrix assisted laser desorption quadrupole-time-of-flight mass spectrometry (MALDI QqTOF) with an Applied Biosystems QSTAR XL hybrid quadrupole-time-of-flight (QqTOF) mass spectrometer equipped with a vacuum MALDI source. Electrochemical measurements were performed under argon using an EG&G Princeton Applied Research model 273A potentiostat-galvanostat. Polymer films were drop-cast on a Pt button electrode from 1% (w/w) solutions of chloroform or toluene and measurements were made in a three-electrode setup with an Ag wire reference electrode calibrated vs. Fc/Fc^+ and a Pt counter electrode. Absorption was measured on a Cary 500 UV-Vis-NIR spectrophotometer.

X-ray crystallography data were collected at 173 K on a Siemens SMART PLATFORM equipped with A CCD array detector and a graphite monochromator utilizing MoK radiation (0.71073 Å). Cell parameters were refined using up to 8192 reflections. A full sphere of data (1850 frames) was collected using the scan method (0.3 frame width). The first 50 frames were re-measured at the end of data collection to monitor instrument and crystal stability (maximum correction on I was <1%). Absorption corrections by integration were applied based on measured indexed crystal faces. The structure was solved by the Direct Methods in *SHELXTL6*, and refined using full-matrix least squares. The non-H atoms were treated anisotropically, whereas the hydrogen atoms were calculated in ideal positions and were riding on their respective carbon atoms. The molecules are located on inversion centers thus a half molecule exists in the asymmetric unit. A total of 154 parameters were refined in the final cycle of refinement using 2643 reflections with $I > 2(I)$ to yield R_1 and wR_2 of 2.43% and 6.40%, respectively. Refinement was done using F^2. X-ray diffraction was performed on polymer films using XRD Philips APD 3720.

Differential scanning calorimetry (DSC) scans were run on a DuPont 951 instrument using the following temperature program: First an equilibration temperature at −80°C for $PBTB(OC_7H_{15})_2$ and at −65°C for $PBTB(OC_{12}H_{25})_2$ was performed. Then the samples were heated at 10°C/min to 200°C, then cooled down at the same rate to −80°C for $PBTB(OC_7H_{15})_2$ and −65°C for $PBTB(OC_{12}H_{25})_2$, and held at these temperatures for 1 min. Another scan was run

following the same method and the results presented in this paper correspond to this second scan. The samples were run under a blanket of nitrogen.

Quantum chemical calculations were performed using computational program (Gaussian 2003). In order to accommodate the large size of the calculation, it was necessary to use DFT on the heterocycle backbone with OCH_3 side chains. The remainder of the alkyl portion of the side chains was then added in all trans conformation for the HOMO and LUMO energy calculations. The geometry was optimized at the B3LYP/6-31G level and the HOMO and LUMO energies calculated at B3LYP/6-311 + G(2d,p) level.

Solar cells were fabricated on indium tin oxide (ITO) covered glass substrates (Delta Technologies, Rs = 8–12 Ω). The ITO/glass substrates were etched by exposure to aqua regia vapor and subsequently cleaned in an ultrasonic bath for 15 min with aqueous sodium dodecyl sulfate (SDS, Fisher scientific), deionized water (Milli-Q), acetone, and isopropanol. The substrates were then treated with oxygen plasma for 15 min in a Plasma Cleaner (HARRICK PDC-32G). Aqueous PEDOT-PSS (Bayer Baytron P VP Al 4083) solution was spin coated at 4000 rpm onto a glass substrate and dried under vacuum for 2–4 h at 150°C. The photoactive layer was then spin-coated and the resulting films were dried under vacuum for 2–3 days at room temperature. Lithium Fluoride (Li:F, 0.5 nm) and Aluminum (Al, 200 nm) were sequentially deposited by thermal evaporation on the photoactive layer. The devices were then encapsulated with epoxy. The active area of the devices was 0.25 cm^2.

The current–voltage (I–V) characteristics were measured with a Keithley SMU 2400 source measurement unit under the illumination of AM 1.5 with an incident power density of 100 mW/cm^2 using a 150 W Xe arc lamp power supply (Oriel instruments). The external quantum efficiency of the photovoltaic devices was also evaluated by measuring the incident photon to current efficiency (IPCE %). In this case device pixels were irradiated with monochromatic light from a 75 W tungsten-halogen lamp. Here, the light from the lamp was passed through a monochromator (Instruments SA Inc., 1200VIS), and the wavelength of light was selected. The power output of the lamp was recorded at 10 nm wavelength intervals between 350 and 750 nm using a UDT instruments S350 Power-Energy Meter equipped with a UDT 221 Silicon Sensor Head. The current response under short circuit conditions was then recorded for each pixel at 10 nm intervals using a Keithley 2400 SMU (positive lead to ITO and negative lead to aluminum).

2.2 Monomer Synthesis

1,4-Dibromo-2,5-diheptoxybenzene, (18, 21) 1,4-dibromo-2,5-didodecyloxy-benzene, (18) 2-(trimethylstannyl)thiophene, (22) 1,4-bis(2-thienyl)-2,5-diheptoxy-benzene, (18) and 1,4-bis(2-thienyl)-2,5-didodecyloxybenzene (18) were synthesized as previously reported.

2.2.1 1,4-Bis(2-(5-bromo)thienyl)-2,5-diheptoxybenzene (**1a**)

Compound 1,4-bis(2-thienyl)-2,5-diheptoxybenzene (2.07 g, 4.40×10^{-3} mol) was dissolved in anhydrous DMF (125 mL) under argon and this yellow slurry was cooled to 0 °C. Freshly recrystallized NBS (1.66 g, 9.40×10^{-3} mol) was added in small portions. The reaction was left at 0°C for 3 h. It was then warmed at room temperature and stirred overnight. Deionized water (300 mL) was added to the yellow slurry and the mixture was extracted with diethyl ether. The organic phase was washed with brine, dried over $MgSO_4$ and filtered through a Büchner funnel. The solvent was evaporated and a yellow solid was collected and dried under vacuum. Pure yellow crystals, 1.99 g (72%) were obtained by recrystallizations from ethanol/benzene (2/1) and ethanol/THF (2/1) [mp = 104–105°C]. ^{1}H-NMR ($CDCl_3$, ppm): $\delta = 7.25$ (d, 1H), 7.16 (s, 1H), 7.04 (d, 1H), 4.07 (t, 2H), 1.91 (p, 2H), 1.52 (m, 2H), 1.34 (m, 6H), 0.91 (t, 3H). ^{13}C-NMR ($CDCl_3$): $\delta = 149.30$, 140.70, 129.50, 124.80, 122.80, 113.40, 111.60, 70.06, 31.98, 29.53, 29.27, 26.39, 22.85, 14.35. Anal. Calcd for $C_{28}H_{36}Br_2O_2S_2$: C, 53.51, H, 5.77. Found: C, 53.64, H, 5.77. HRMS $C_{28}H_{36}Br_2O_2S_2$: Calcd: 626.0523; Found: 626.0524.

2.2.2 1,4-Bis(2-(5-bromo)thienyl)-2,5-didodecyloxybenzene (**1b**)

Compound **1b** was prepared according to the procedure described for **1a** utilizing 1,4-bis(2-thienyl)-2,5-didodecyloxybenzene (8.86 g, 1.45×10^{-2} mol), anhydrous DMF (350 mL) and freshly recrystallized NBS (5.39 g, 3.05×10^{-2} mol). After recrystallizations from ethanol/benzene (2/1), ethanol/THF (2/1), and methanol/THF (2/1), 9.54 g (86%) of pure yellow crystals were obtained [mp = 101–103°C]. ^{1}H-NMR ($CDCl_3$, ppm): $\delta = 7.25$ (d, 1H), 7.17 (s, 1H), 7.04 (d, 1H), 4.08 (t, 2H), 1.92 (p, 2H), 1.52 (m, 2H), 1.27 (m, 16H), 0.89 (t, 3H). ^{13}C-NMR ($CDCl_3$): $\delta = 149.20$, 140.60, 129.49, 124.80, 122.80, 113.20, 111.61, 70.06, 32.17, 29.92, 29.89, 29.84, 29.80, 29.61, 26.44, 22.94, 14.40. Anal. Calcd. for $C_{38}H_{56}Br_2O_2S_2$: C, 59.37, H, 7.34. Found: C, 59.67, H, 7.54. HRMS $C_{38}H_{56}Br_2O_2S_2$: Calcd: 766.2088; Found: 766.2098.

2.3 Polymer Synthesis

2.3.1 Poly(1,4-bis(2-thienyl)-2,5-diheptoxybenzene) (**2a**)

$Ni(COD)_2$ (1.04 g, 3.78×10^{-3} mol) and Bpy (49.50×10^{-2} g, 3.17×10^{-3} mol) were combined in a Schlenk flask under argon and dissolved in anhydrous DMF (30 mL). A solution of 1,5-cyclooctadiene (0.39 mL, 3.12×10^{-3} mol) was quickly added via a syringe. The purple solution was warmed to 60°C for 40 min and slowly added to a 50 mL solution of 1,4-bis[2-(5-bromo)thienyl]-2,5-diheptoxybenzene (1.98 g, 3.15×10^{-3} mol) in anhydrous DMF. The color turned immediately red. The reaction was maintained at 60°C for

48 h in the dark. The solution was cooled to room temperature and poured into methanol (1L) yielding a red precipitate which was filtered through a Soxhlet thimble. The precipitate was purified by Soxhlet extraction for 24 h with methanol and 30 h with hexane. The polymer was fractionated with toluene. The toluene was evaporated under reduced pressure to afford 0.82 g (55%) of red solid. ^{1}H NMR ($CDCl_3$, ppm): $\delta = 7.50$ (Th-H), 7.21 (Ar-H), 7.05 (TH-H), 4.15 (OCH_2), 1.95 (OCH_2CH_2), 1.32 (CH_2), 0.90 (CH_3). GPC analysis: $M_n = 4{,}960$, $M_w = 6{,}340$, PDI = 1.28.

2.3.2 Poly(1,4-bis(2-thienyl)-2,5-didodecyloxybenzene) (2b)

Polymer **2b** was prepared according to the procedure described for **2a** utilizing $Ni(COD)_2$ (8.61×10^{-2} g, 3.13×10^{-3} mol), Bpy (4.90×10^{-1} g, 3.14×10^{-3} mol), anhydrous DMF (50 mL), 1,5-cyclooctadiene (0.32 mL, 2.62×10^{-3} mol) and 1,4-bis[2-(5-bromo)thienyl]-2,5-didodecyloxybenzene (2.00 g, 2.60×10^{-3} mol). The polymerization solution was stirred at 60°C for 24 h. A red solid (6.36×10^{-1} g, 40%) was recovered after Soxhlet extraction in toluene. ^{1}H NMR ($CDCl_3$, ppm): $\delta = 7.50$ (Th-H), 7.21 (Ar-H), 7.05 (Th-H), 4.13 (OCH_2), 1.96 (OCH_2CH_2), 1.27 (CH_2), 0.87 (CH_3). GPC analysis: $M_n = 2{,}945$, $M_w = 3{,}950$, PDI = 1.34.

3 Results and Discussion

3.1 Monomer Synthesis

1,4-Dibromo-2,5-dialkoxybenzenes were prepared by Williamson etherification of 1,4-dibromo-2,5-dihydroxybenzene with the corresponding alkyl halide. The synthesis of the brominated 1,4-bis(2-thienyl)-2,5-diheptoxybenzene $BTB(OC_7H_{15})_2$ and 1,4-bis(2-thienyl)-2,5-didodecyloxybenzene $BTB(OC_{12}H_{25})_2$ monomers started by the deprotonation of thiophene with *n*-butyllithium followed by reaction with trimethylstannyl chloride to give 2-(trimethylstannyl)-thiophene. The 1,4-bis(2-thienyl)-2,5-dialkoxybenzenes were obtained by the Stille coupling of 1,4-dibromo-2,5--dialkoxybenzene with 2-(trimethylstannyl)thiophene. Bromination of $BTB(OR)_2$ was accomplished by the addition of NBS (72% and 86% for R = C_7H_{15} and $C_{12}H_{25}$, respectively) to yield monomers **1**.

3.2 Polymer Synthesis

Polymerization of the monomers (**1a** and **1b**) was carried out via Yamamoto coupling as seen in Scheme 2 in a dry box (23–25). The zerovalent nickel reagent, bis (1,5-cyclooctadiene)nickel ($Ni(COD)_2$) was mixed with one molar equivalent of 2,2′-bipyridiyl (Bpy) in order to generate the active reagent Ni(COD)(Bpy). An additional equivalent of 1,5-cyclooctadiene (COD) is added to the mixture as COD is observed to drive the reaction via the suspected activation of the aryl-Ni(II)-aryl species by coordination to the nickel, thus driving the reductive elimination and aryl-aryl bond formation (23). The addition order of the monomer and the nickel reagent is important in order to maximize the molecular weights. Indeed, as seen in the literature, the reverse order results in the formation of a $L_m(Br)Ni\text{-}Ar\text{-}Ni(Br)L_m$ complex due to the high ratio between the Ni(0)reagent and the monomer. This complex decomposes or hydrolyzes easily giving rise to termination of the polymer chain.

The polymers were characterized by ^{1}H-NMR, GPC and MALDI-MS, cyclic voltammetry, and elemental analysis. The corresponding GPC and electrochemistry results are summarized in Table 1. Polymer chains of reasonable size (*ca.* 20–30 rings) were obtained for the PBTB derivatives. The polymers exhibit a solubility of about 7 mg/mL in toluene, which allows preparation of high quality films via spray-casting. The molar masses of the repeat units were observed by MALDI-MS in a terthiophene matrix (26). From the spacing of the mass spectra, values of 468 g/mol for $PBTB(OC_7H_{15})_2$ shown in Figure 1 and 609 g/mol for $PBTB(OC_{12}H_{25})_2$ were observed, as expected for the molecular weights of the repeat units. End groups for the primary ion series are hydrogen. There are also weaker ion series that correspond to species with hydrogen-bromine and bromine-bromine groups.

3.3 Primary Structure

As shown in Figure 2, comparison of the ^{1}H-NMR spectra of monomer $Br_2(BTB(OC_{12}H_{25})_2)$ and polymer $PBTB(OC_{12}H_{25})_2$ show a similar pattern except for several peaks in the aromatic region (6.8–7.6 ppm). In that region, three peaks were observed for the monomer at 7.25 ppm (d, 2H), 7.17 ppm (s, 2H), and 7.04 ppm (d, 2H) and assigned as H_a, H_c and H_b, respectively. The proton peaks of the corresponding polymer $PBTB(OC_{12}H_{25})_2$ were observed at 7.5 ppm, 7.21 ppm, and 7.05 ppm and were also assigned as H_a, H_c

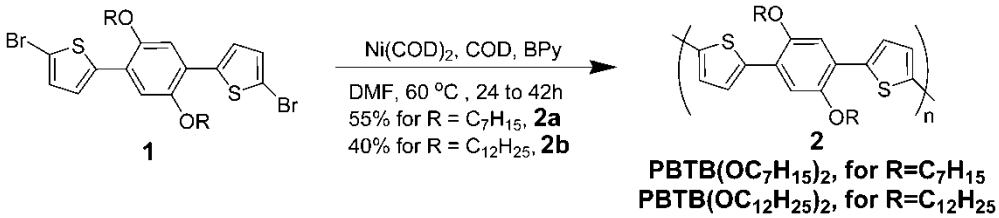

Sch. 2. Polymerization of isoregic thienylene-phenylene polymers.

Table 1. Summarized gel permeation chromatography[a] and cyclic voltammetry[b] results for isoregic thienylene-phenylene polymers

Samples	M_n (g/mol)	M_w (g/mol)	PDI	Average # rings[c]	$E_{p,a}$ (V)	$E_{p,c}$ (V)	$E_{1/2}$ (V)
PBTB(OC_7H_{15})$_2$	4,960	6,340	1.3	29	0.09	0.47	0.28
PBTB($OC_{12}H_{25}$)$_2$	2,945	3,950	1.3	17	0.24	0.84	0.54

[a]Molecular weights and polydispersity indexes (PDI) were estimated by size exclusion chromatography against polystyrene standards.
[b]Potential vs. Fc/Fc^+, 0.1 M TBAP in propylene carbonate and at scan rate of 100 mV/s.
[c]Average number of aromatic rings per chain.

and H_b after coupling between two thiophene rings and is consistent with the repeat unit structure shown in Scheme 2.

3.4 Electronic Spectra

In Figure 3A, the absorption spectra of the monomers and polymers in toluene are shown. The absorption maximum ($\lambda_{max,m}$) of both Br_2(BTB($OC_{12}H_{25}$)$_2$) and Br_2(BTB(OC_7H_{15})$_2$) were observed at 376 nm. The absorption peaks ($\lambda_{max,p}$) of PBTB($OC_{12}H_{25}$)$_2$ and PBTB(OC_7H_{15})$_2$ in toluene appeared at 463 nm ($\varepsilon = 22{,}700\ Lmol^{-1}cm^{-1}$) and 473 nm ($\varepsilon = 7240\ Lmol^{-1}cm^{-1}$), respectively. The corresponding peak maximum shifts from monomer ($\Delta\lambda_{max} = \lambda_{max,p} - \lambda_{max,m}$) after polymerization are consequently 87 and 97 nm indicating the increased conjugation length of the polymers. The 10 nm difference in λ_{max} between the two polymers may be attributed to steric interactions of the long -$OC_{12}H_{25}$ pendant group that induces a slightly larger torsional angle along the conjugated chain.

In the solid state, the polymers exhibit absorption maxima at 440 nm and 455 nm for PBTB($OC_{12}H_{25}$)$_2$ and PBTB(OC_7H_{15})$_2$, respectively (Figure 3B, measured on ITO/Glass substrate). Absorption shoulders were observed for all the polymer films, at 474 nm and 526 nm for PBTB($OC_{12}H_{25}$)$_2$ and at 488 nm and 531 nm for PBTB(OC_7H_{15})$_2$. The peak differences observed between solution and the solid state (including shoulders) are attributed to the conformational changes. On a solid substrate, the polymers tend to planarize extending their conjugation by restricting the free rotation of the backbone. While PBTB(OC_7H_{15})$_2$ has a bit more red absorption, the absorption edges were observed at 563 nm, and 566 nm for both

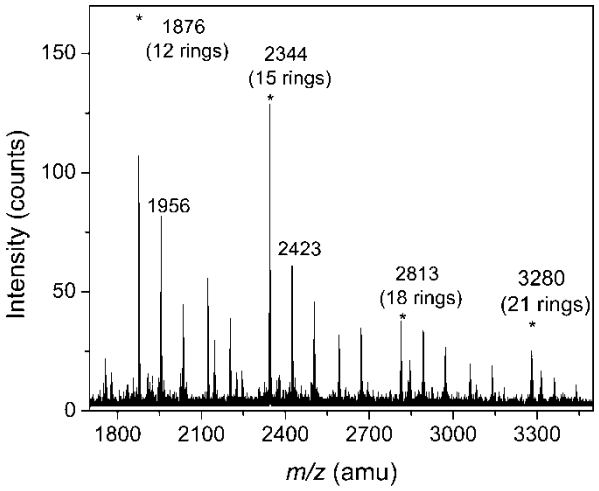

Fig. 1. MALDI-MS for PBTB(OC_7H_{15})$_2$. Spacing was observed to be 468 amu – The isotopes are resolves and the peak labels indicate the most intense peak of each isotope cluster.

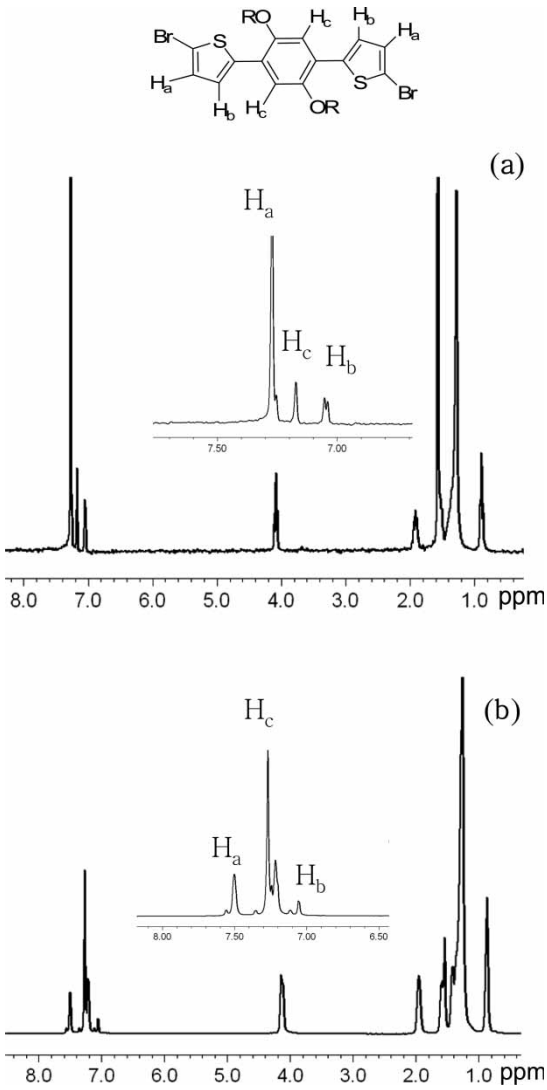

Fig. 2. ^{1}H-NMR for (a) monomer Br_2(BTB($OC_{12}H_{25}$)$_2$) and (b) polymer BTB($OC_{12}H_{25}$)$_2$ in $CDCl_3$.

polymers yielding an electronic band gap of 2.1 eV. The similarity of these spectra suggests that both polymers have a sufficiently high degree of polymerization and that the small changes are likely due to packing effects.

3.5 Spectroelectrochemistry

The spectroelectrochemical results for $PBTB(OC_7H_{15})_2$ are depicted in Figure 4 as the potential was stepped from -0.5 V to $+0.9$ V showing an excellent Gator color switching between orange and blue from the neutral to the oxidized state. In the oxidized state, the polymer film showed a stable and broad absorption over the visible and near IR spectral regions attributed to the delocalized charge carriers along the conjugated polymer backbone. For $PBTB(OC_{12}H_{25})_2$ (not shown), the potential was stepped from -0.75 V to 0.75 V. In the oxidized state, $PBTB(OC_{12}H_{25})_2$ showed two well resolved absorption bands, one in the visible (650–700 nm) and another in the near IR spectral regions (1000–1100 nm), giving rise to a blue-grey color in the oxidized state and a pale orange color in the neutral state.

The combination of the spectroelectrochemical and electrochemical experiments (presented in Table 1) allowed us to evaluate the positions of the HOMO and LUMO bands of the polymers. The polymers were deposited on Pt button electrodes and cyclic voltammograms were recorded in 0.1 M TBAP/propylene carbonate solutions. The onset of oxidation of $PBTB(OC_7H_{15})_2$ is about 0.25 V and the $E_{1/2}$ is 0.29 V. These results correlate with a HOMO energy of approximately 5.4 eV based on the Fc/Fc^+ reference electrode at 0.38 V vs. SCE (14). Combining this with the optically determined band gap of 2.1 eV, yields a LUMO energy of 3.3 eV. The onset of oxidation for $PBTB(OC_{12}H_{25})_2$ is more positive, around 0.35 V, resulting in an estimated HOMO level at about 5.5 eV and places the LUMO level at 3.4 eV. The band structure and computational details will be discussed later.

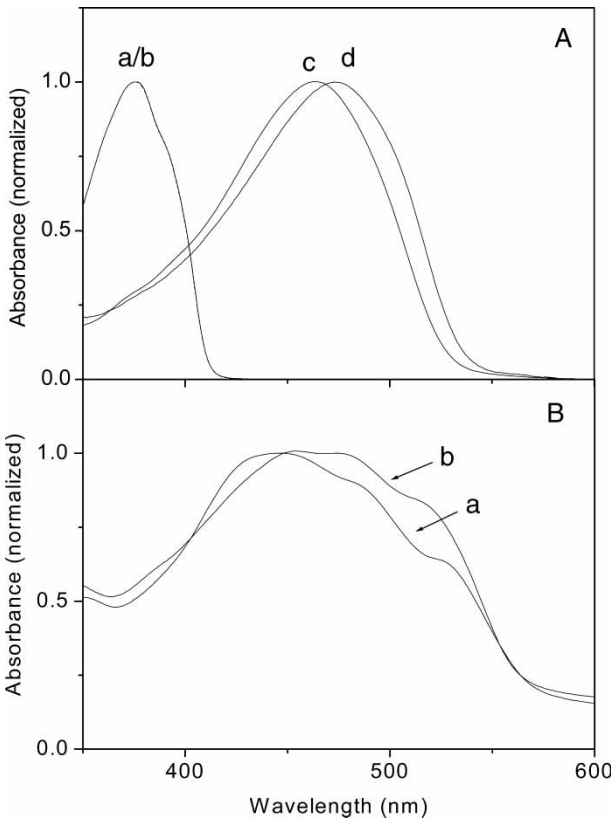

Fig. 3. Absorption spectra of monomers and polymers. (A): solution state (in toluene) absorbance [(a) $Br_2(BTB(OC_{12}H_{25})_2)$, (b) $Br_2(BTB(OC_7H_{15})_2)$, (c) $PBTB(OC_{12}H_{25})_2$, (d) $PBTB(OC_7H_{15})_2$] and (B): solid state absorbance [(a) $PBTB(OC_{12}H_{25})_2$ and (b) $PBTB(OC_7H_{15})_2$].

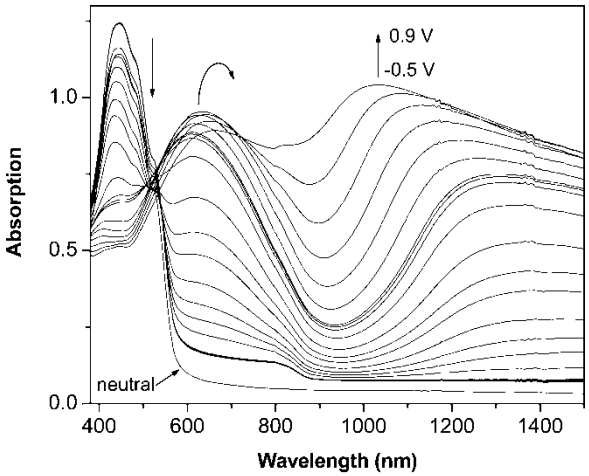

Fig. 4. UV/Vis/NIR spectroelectrochemical spectra of $PBTB(OC_7H_{15})_2$. Potential (V) *vs.* $Fc./Fc^+$.

3.6 X-ray Crystallography

The crystal structure of the monomer $Br_2(BTB(OC_7H_{15})_2)$ was measured and Figure 5(a) shows a perspective view, while Figure 5(b) shows the crystalline unit cell to illustrate molecular packing. The torsional angle between the phenylene and thiophene units, and the distance between facing rings were observed to be 20.8° and 5.79 Å, respectively. This molecule crystallizes in the monoclinic space group C2/c with the two alkoxy chains found to be coplanar with the phenyl rings in the molecule. As seen in Figure 5(b), there is an effective stacking of adjacent molecules in full register. While this is larger than what is desired for a high degree of overlap, and is also larger than the van der Waals separation of two bromines of 3.7 Å, the structure suggests that intermolecular charge transfer via hopping may be possible in the corresponding polymers should similar packing be attained.

X-ray diffraction was performed on polymer films which had been annealed at 180°C for 4 h for $PBTB(OC_{12}H_{25})_2$ and at 220°C for 4 h for $PBTB(OC_7H_{15})_2$. In Figure 6, the X-ray diffraction pattern of $PBTB(OC_{12}H_{25})_2$ is shown and

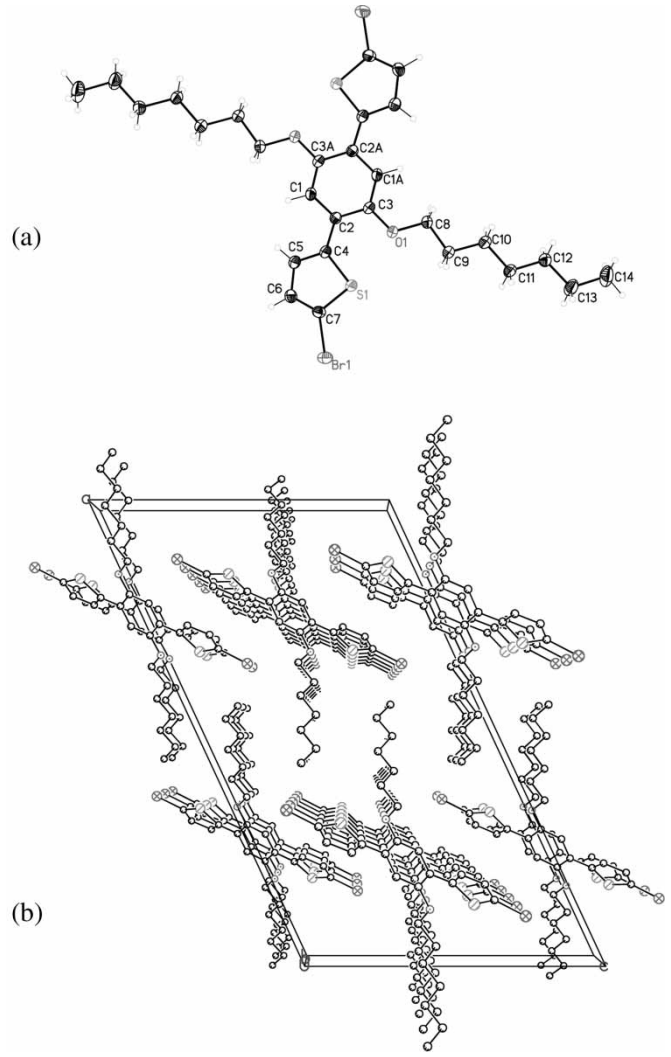

Fig. 5. Crystal structure of monomer $Br_2(BTB(OC_7H_{15})_2)$. Distance between facing rings was found to be 5.79 Å and the torsional angle between benzene and thiophene was observed to be 20.8°.

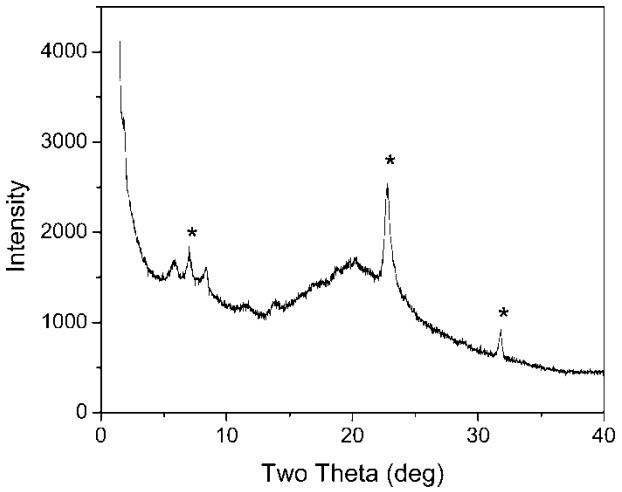

Fig. 6. X-ray diffraction patterns of annealed and cast $PBTB(OC_{12}H_{25})_2$ on glass, from scans of intensity *vs.* 2θ.

demonstrates the semi-crystalline nature of the polymer. A strong peak at 22.8° is observed and is attributed to coplanar stacking of the aromatic chains with a spacing of 3.83 Å, closer than what was observed in the monomer. J. Ruiz et al. (18) reported consistent X-ray diffraction pattern, where sharp diffraction patterns on the order of 3–4 Å were observed. Well-resolved diffraction peaks are observed at low angles corresponding to interlayer spacing of 10.45, 12.59, and 14.99 Å and suggest that lamellar structures are forming. In J. Ruiz's work, well resolved diffraction patterns that was assigned to the interlayer spacings of 12.44, 12.95, and 20.35 Å are shown. $PBTB(OC_7H_{15})_2$ also exhibits long-range order with diffraction peaks at 9.51 and 12.5 Å.

3.6 Thermal Analysis

Order in these polymers was also studied by differential scanning calorimetry (DSC) as seen in Figure 7. The symmetrically derivatized polymers exhibit two endothermic transitions. Previous work on this type of molecule has shown that the highest transition T_2 is attributed to an isotropic melt of the polymer backbone (18). The temperature of this transition is observed to decrease as the length of the side chains is increased. These results confirm the semi-crystalline nature of the polymers.

3.7 Quantum Chemical Calculations

Quantum chemical calculations are a useful tool for evaluating the relationship between electronic energy levels and molecular structure. Simple molecular structures and minimal effective molecular weight are usually required for this type of measurement in order to reduce possible misinterpretations that can be found in complex and disordered giant molecules (27). Evaluation of the electronic band structure of well ordered molecules such as regioregular poly(3-alkylthiophene) (28) or pentacene (29) with quantum chemical calculations have been reported to detail their high charge carrier mobility.

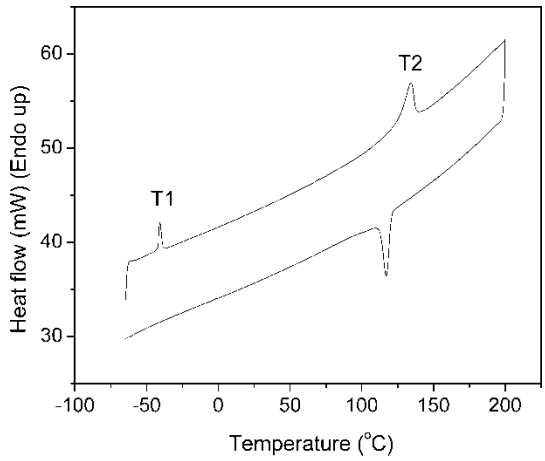

Fig. 7. Reproducible DSC thermogram (2nd scan) of $PBTB(OC_{12}H_{25})_2$ with T1 = −41°C and T2 = 134°C.

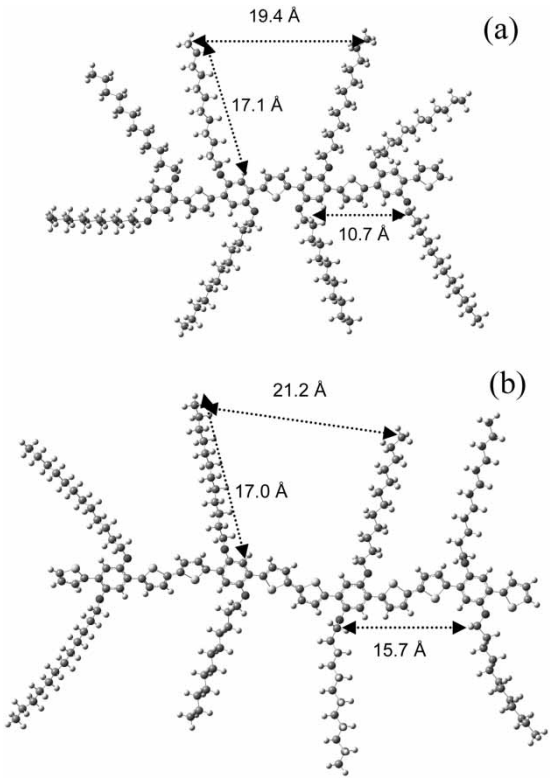

Fig. 8. Geometry optimized structures of (a) PTB($OC_{12}H_{25}$)$_2$ and (b) PBTB($OC_{12}H_{25}$)$_2$. In a series of calculations at the B3LYP/6–31G level, the average inter ring torsion angle of PTB($OC_{12}H_{25}$)$_2$ decreased from 18.5 degrees for two rings to 14.5 degrees for six rings.

The geometry optimized structure of PBTB($OC_{12}H_{25}$)$_2$ having $X_n = 4$ (12 rings) is shown in Figure 8(b). The distance (10.4–15.7 Å) between adjacent side-chains of PBTB($OC_{12}H_{25}$)$_2$ is larger than that (5.9–10.7 Å) of analogous polymer that has a thiophene moiety between alkoxy-substituted phenylene, due to the presence of two thiophenes that act as spacers between phenylenes. This feature lowers the torsion angle, allows facing rings to pack on top of one another better, and consequently adjacent polymer chains can gain a quasi-planar configuration. In the case of PBTB(OC_7H_{15})$_2$, it is expected that the shorter length of the side chain may help the polymer backbones to be closer to one another and have an impact on the intramolecular and intermolecular photoinduced charge transport properties. Close packing of the polymer chains is an important feature for charge carrier delocalization in organic electronics.

Table 2. HOMO-LUMO energies and band gap values of PBTB(OC_7H_{15})$_2$ and PBTB($OC_{12}H_{25}$)$_2$ obtained from spectroscopy, electrochemistry, and quantum chemical calculations[a]

Samples	LUMO (eV)	HOMO (eV)	Band gap (eV)
PBTB(OC_7H_{15})$_2$	3.3 (2.29)	5.4 (4.97)	2.1 (2.68)
PBTB($OC_{12}H_{25}$)$_2$	3.4 (2.29)	5.5 (4.97)	2.1 (2.68)

[a]values in parentheses are calculated using DFT (Gaussian 03). HOMO and LUMO energies were calculated using B3LYP/6–311 + G(2d,p) with geometries optimized at B3LYP/6–31G for six backbone rings with OCH_3 side chains and then the remainder of the alkyl portion of the side chains added in an all trans conformation.

In Scheme 3, the electronic band structure of the components in a PV device is illustrated. A simplified representation of the HOMO-LUMO energies of PBTB($OC_{12}H_{25}$)$_2$ is depicted on the left side of Scheme 3. The isosurfaces of HOMO-LUMO charge density are depicted as well, illustrating the aromatic and quinoid characteristics of the polymer. As seen in Table 2, the density functional theory (DFT) determined HOMO and LUMO energies show a trend consistent

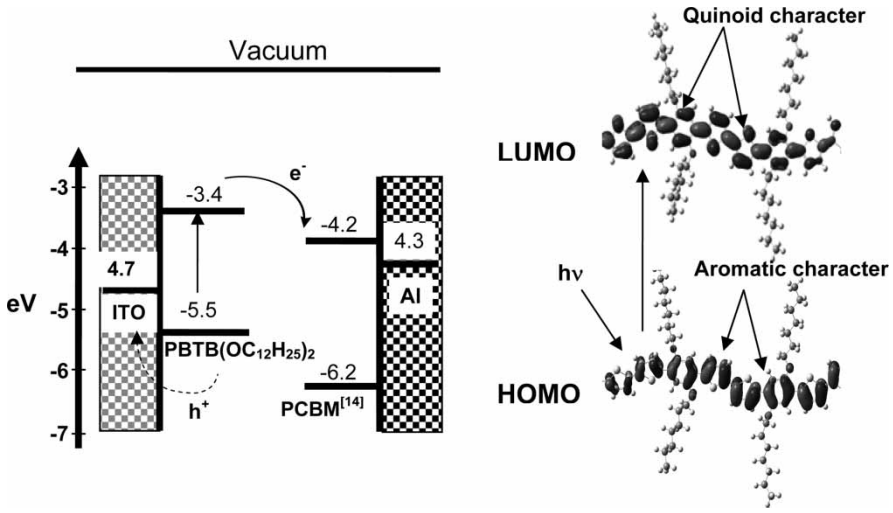

Sch. 3. Simplified structure of the HOMO-LUMO energies of PBTB($OC_{12}H_{25}$)$_2$ and corresponding illustration of aromatic and quinoid characteristics of the polymer.

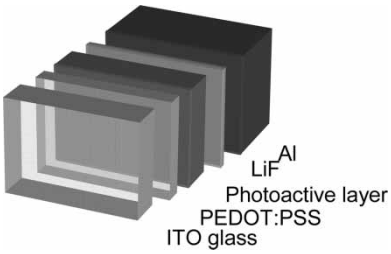

Sch. 4. Schematic of a photovoltaic device (PVD).

with the electrochemical and spectroscopic data, though the absolute values vary to a greater extent compared to the experimental measures. Comparing PBTB(OC_7H_{15})$_2$ and PBTB($OC_{12}H_{25}$)$_2$ the calculated HOMO and LUMO energies are identical, suggesting that the differences seen experimentally are due to molecular conformational effects such as interchain packing rather than an electron donating or withdrawing effects based on the length of the side chains. The combination of all the studies including quantum chemical calculations, electrochemistry, and spectroscopy are consistent with one another in developing an understanding of the polymer's electronic properties. The comprehensive understanding on the electronic properties along with structural variation leads us to utilize the polymers for converting light energy into electricity in polymer/PCBM solar cells.

3.8 PCBM: Polymer Photovoltaic Cells

Based on the characteristics of the polymers, bulk heterojunction PCBM based solar cells have been fabricated with the configuration shown in Scheme 4. The polymer/PCBM composition ratio for fabricating the PVDs was 1/4 by weight and the thickness of the photoactive layer was *ca.* 45 nm. The composition ratio used recognized as effective for polymer solar cells, while post thermal-treated P3HT/PCBM solar cells have been reported to show the best PV properties in a range of polymer/PCBM composition ratio of 2.4/4 to 4/4 by weight. The P3HT is regioregular and attains long range order after thermal treatment, for which the well-ordered polymer can contribute to transfer photoinduced charge for maximizing PV performance of the polymer/PCBM solar cells. In Figure 9 and Table 3, representative I-V characteristic curves and corresponding PVD data are presented. As an example, PBTB(OC_7H_{15})$_2$/PCBM based PVD showed AM1.5 efficiencies of ~0.6% with a short circuit current of 2.49 mA/cm^2, an open circuit voltage of 0.74 V, and a fill factor of 0.32. PBTB($OC_{12}H_{25}$)$_2$ showed AM1.5 efficiency of 0.48%, with the decreased efficiency attributed to the lower current densities (from 2.49 to 1.59 mA/cm^2). The external quantum efficiencies for the solar cells are illustrated in Figure 10. PBTB(OC_7H_{15})$_2$/PCBM and PBTB($OC_{12}H_{25}$)$_2$/PCBM based PVDs exhibit IPCEs around 16% at 410 nm. Overall, both PBTB(OC_7H_{15})$_2$ and PBTB($OC_{12}H_{25}$)$_2$ demonstrate their potential for use in organic PVDs harvesting incident light of the mid-range energy.

Table 3. Summarized I-V characteristics of isoregic conjugated polymer/PCBM based solar cells[a]

Photosensitizer	η (%)	FF	V_{oc} (V)	I_{sc} (mA/cm^2)
PBTB(OC_7H_{15})$_2$	0.59	0.32	0.74	2.49
PBTB($OC_{12}H_{25}$)$_2$	0.48	0.39	0.76	1.59

[a]Composition: 1/4 by wt (Polymer/PCBM) and concentration of solution applied: 30 mg/ml.
[b]Thickness of photoactive layer: about 45 nm.

4 Conclusions

Regiosymmetric conjugated oligomers and polymers have been synthesized by Yamamoto coupling polymerization

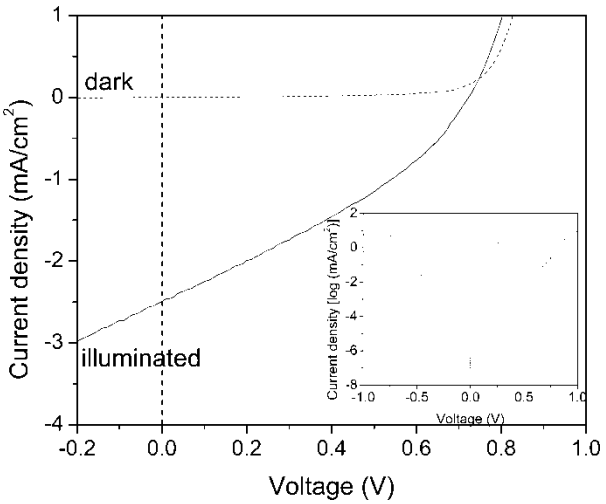

Fig. 9. I-V characteristics of PBTB($OC_{12}H_{25}$)$_2$/PCBM based solar cells. Composition ratio is 1/4 by weight.

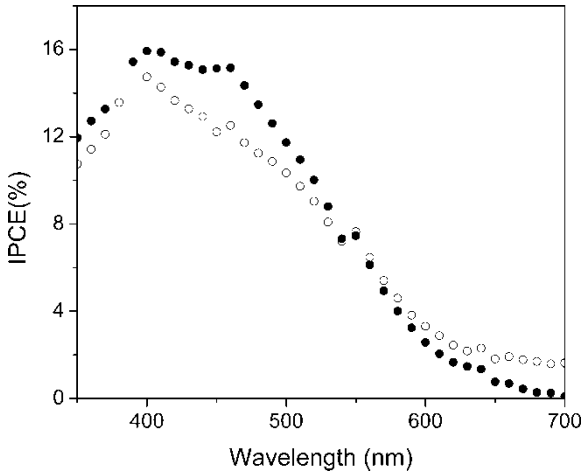

Fig. 10. IPCEs of PBTB($OC_{12}H_{25}$)$_2$/PCBM solar cell (•) and PBTB(OC_7H_{15})$_2$/PCBM solar cell (○). Composition ratio is 1/4 by weight.

using $Ni(COD)_2$. The HOMO and LUMO energy levels of the materials, as well as their PV performance have been evaluated and indicate these materials provide a strong PV effect. Computer-aided simulation and spectroelectrochemistry were helpful determining the electronic properties of the polymers and give us good insight for understanding the role of the molecular structure in organic electronics. This class of polymer can efficiently harvest incident light in the mid-visible energy range and could be used in *multi*-light harvesting sensitizer based solar cells.

5 Acknowledgements

We gratefully acknowledge the AFOSR (FA9550-06-1-0192) and EIC Laboratories (NNC05CB23C) for support of this work. T.D.M. wishes to thank the NSF for funding (CHE-0074884).

6 References

1. Heeney, M., Bailey, C., Giles, M., Shkunov, M., Sparrowe, D., Tierney, S., Zhang, W. and McCulloch, I. (2004) *Macromolecules*, **37**, 5250–5256.
2. Locklin, J., Li, D., Mannsfeld, S.C.B., Borkent, E.-J., Meng, H., Advincula, R. and Bao, Z. (2005) *Chem. of Mater.*, **17**, 3366–3374.
3. Tseng, R.J., Huang, J., Ouyang, J., Kaner, R.B. and Yang, Y. (2005) *Nano Lett.*, **5**, 1077–1080.
4. Christie, A.M., Lilley, S.J., Staunton, E., Andreev, Y.G. and Bruce, P.G. (2005) *Nature*, **433**, 50–53.
5. Diederich, L., Barborini, E., Piseri, P., Podesta, A., Milani, P., Schneuwly, A. and Gallay, R. (1999) *Appl. Phys. Lett.*, **75**, 2662–2664.
6. Peumans, P., Uchida, S. and Forrest, S.R. (2003) *Nature*, **425**, 158–162.
7. Huynh, W.U., Dittmer, J.J. and Alivisatos, A.P. (2002) *Science*, **295**, 2425–2427.
8. Lindner, S.M. and Thelakkat, M. (2004) *Macromolecules*, **37**, 8832–8835.
9. Veinot, J.G.C. and Marks, T.J. (2005) *Acc. Chem. Res.*, **38**, 632–643.
10. Argun, A.A., Aubert, P.-H., Thompson, B.C., Schwendeman, I., Gaupp, C.L., Hwang, J., Pinto, N.J., Tanner, D.B., MacDiarmid, A.G. and Reynolds, J.R. (2004) *Chem. Mater.*, **16**, 4401–4412.
11. Sariciftci, N.S., Smilowitz, L., Heeger, A.J. and Wudl, F. (1992) *Science*, **258**, 1474–1476.
12. (a) Coakley, K.M. and McGehee, M.D. *Chem. Mater.*, 2004, **16**, 4533–4542; (b) Hoppe, H. and Sariciftci, N.S. (2004) *J. Mater. Res.*, **19**, 1924–1945; (c) Brabec, C.J., Sariciftci, N.S. and Hummelen, J.C. (2001) *Adv. Funct. Mater.*, **11**, 15–26.
13. (a) Roncali, J. *Chem. Rev.*, 1997, **97**, 173–205; (b) van Mullekom, H.A.M., Vekemans, J.A.J.M., Havinga, E.E. and Meijer, E.W. (2001) *Mater. Sci. Eng.*, **32**, 1–40.
14. (a) Kim, Y.G., Thompson, B.C., Iyengar, N.A., Padmanaban, G., Ramakrishnan, S. and Reynolds, J.R. (2003) *J. Mater. Res.*, **20**, 3188–3198; (b) Thompson, B.C., Kim, Y.G. and Reynolds, J.R. (2005) *Macromolecules*, **38**, 5359–5362.
15. (a) Reyes-Reyes, M., Kim, K. and Carroll, D.L. (2005) *Appl. Phys. Lett.*; (b) Li, G., Shrotriya, V., Huang, J., Yao, Y., Moriarty, T., Emery, K. and Yang, Y. (2005) *Nat. Mater.*, **4**, 864–868; (c) Ma, W., Yang, C., Gong, X., Lee, K. and Heeger, A.J. (2005) *Adv. Funct. Mater.*, **15**, 1617–1622.
16. (a) Galand, E., Kim, Y.G., Jones, A.G., Mwaura, J.K., McCarley, T.D. and Reynolds, J.R. (2006) *Macromolecules*, **39**, 9132–9142; (b) Thompson, B.C., Kim, Y.G., McCarley, T.D. and Reynolds, J.R. (2006) *J. Am. Chem. Soc.*, **128**, 12714–12725; (c) Reeves, B.D., Grenier, C.R.G., Argun, A.A., Cirpan, A., McCarley, T.D. and Reynolds, J.R. (2004) *Macromolecules*, **37**, 7559–7569; (d) Welsh, D.M., Kleoner, L.J., Madrigal, L., Pinto, M.R., Thompson, B.C., Schanze, K.S., Abboud, K.A., Powell, D. and Reynolds, J.R. (2002) *Macromolecules*, **35**, 6517–6525.
17. Wang, F., Wilson, M.S., Rauh, R.D., Schottland, P., Thompson, B.C. and Reynolds, J.R. (2000) *Macromolecules*, **33**, 2083–2091.
18. Ruiz, J.P., Dharia, J.R., Reynolds, J.R. and Buckley, L.J. (1992) *Macromolecules*, **25**, 849–860.
19. (a) Bao, Z., Chan, W.K. and Yu, L. (1995) *J. Am. Chem. Soc.*, **117**, 12426–12435; (b) Bao, Z., Chan, W. and Yu, L. (1993) *Chem. Mater.*, **5**, 2–3.
20. Yamamoto, T. (1999) *Bull. of the Chem. Soc. of Jp.*, **72**, 621–638.
21. Irvin, J.A. and Reynolds, J.R. (1998) *Polymer*, **39**, 2339–2347.
22. Pratt, J.R., Pinkerton, F.H. and Thames, S.F. (1972) *J. Org. Chem.*, **38**, 29–36.
23. (a) Yamamoto, T., Wakabayahi, S. and Osakada, K. (1992) *J. Organometallic Chem.*, **428**, 223–237; (b) Zhang, Z.B.F.M., Tang, H.Z., Motonaga, M. and Torimitsu, K. (2002) *Macromolecules*, **35**, 1988–1990.
24. Semmelhack, M.F.H.P., Jones, L.D., Keller, L., Mendelson, L., Ryono, L.S., Smith, J.G. and Stauffer, R.D. (1981) *J. Am. Chem. Soc.*, **103**, 6460–6471.
25. Yamamoto, T. (1999) *Bull. Chem. Soc. Jpn.*, **72**, 621–638.
26. (a) McCarley, T.D., Noble, C.O., DuBois, C.J. and McCarley, R.L. *Macromolecules*, 2001, **34**, 7999–8004; (b) McCarley, T.D., McCarley, R.L. and Limbach, P.A. (1998) *Anal. Chem.*, **70**, 4376–4379.
27. Zheng, G., Clark, S.J., Brand, S. and Abram, R.A. (2004) *J. Phys.: Condensed Matter*, **16**, 8609–8620.
28. Hutchison, G.R., Ratner, M.A. and Marks, T.J. (2005) *J. Phys., Chem. B*, **109**, 3126–3138.
29. Bredas, J.L., Beljonne, D., Cornil, J., Calbert, J.P., Shuai, Z. and Silbey, R. (2001) *Synth. Met.*, **125**, 107–116.